

# Global effects of different types of land use and land cover changes on near-surface air temperature



Linfei Yu<sup>a,b</sup>, Guoyong Leng<sup>a,b,\*</sup>

<sup>a</sup> Key Laboratory of Water Cycle and Related Land Surface Processes, Institute of Geographic Sciences and Natural Resources Research, Chinese Academy of Sciences, Beijing 100101, China

<sup>b</sup> University of Chinese Academy of Sciences, Beijing 100049, China

## ARTICLE INFO

**Keywords:**  
 Land cover/use change  
 Climate effect  
 Land state change  
 Land transition  
 Land management

## ABSTRACT

Understanding the climate effect of land use and land cover change (LULCC) is critical for guiding human activities towards environmental sustainability. Previous studies have reported the climate effects of global deforestation, vegetation greening and crop cultivation changes. However, the contribution of each type of land state, land transition and land management to LULCC's climate effects remain underexamined. In this study, we estimated global biophysical temperature effects of LULCC using CMIP6 climate models, with special attention on the relative contribution (RC) of 12 land state changes, 113 land transitions and 10 land managements. The results show a large difference in the simulated LULCC's temperature effect between CESM2 and UKESM1–0–LL, and the two models even disagree in the sign of LULCC's effects in most of northern hemisphere except for autumn. Based on the weighted mean of two models, we found that historical LULCC has exerted a global warming effect at a rate of 0.0025 °C/century, with the largest warming effect in autumn. Spatially, a significant ( $p < 0.05$ ) cooling effect is found from 60°N to 40°N, while the warming trend dominates the areas from 40°N to 30°S. Based on regression modelling, historical changes in forested/non-forested secondary land, urban land and cropland have contributed over 70% to LULCC's temperature effect, with land transitions from secondary land to cropland and from cropland to urban land dominating the climate effect at global scale. For land management, the climate effect of irrigation is larger than that of nitrogen fertilizer application. Furthermore, the application of nitrogen fertilizer for C3 plant has larger impacts compared to C4 plants, while similar effects of irrigation are observed for different types of croplands. Besides, the large difference in temperature effect between CESM2 and UKESM1–0–LL may be the difference in the forestland and cropland changes. Our study calls for explicit examination of the climate effect induced by different types of land state-change, land transition and land management for developing targeted land use policies in the future.

## 1. Introduction

Land-cover change has significantly increased over the last 300 years and, nowadays, more than half of global land areas is perturbed to some degree by humans (Asselen et al., 2013; Houghton and Nassikas, 2017; Li et al., 2020a; Tran et al., 2017). Generally, land Use and Land Cover Changes (LULCC) exert impacts on global climate through various biogeochemical and biophysical mechanisms (Alkama and Cescatti, 2016; Huang et al., 2020; Mahmood et al., 2013). Specifically, LULCC induced changes in the biogeochemical processes could influence climate through altering the distribution and concentration of greenhouse gases (such as CO<sub>2</sub>, CH<sub>4</sub>, N<sub>2</sub>O, etc.), thus changing the chemical

composition of the atmosphere (Song et al., 2018; Chen and Dirmeyer, 2016). For biophysical processes, LULCC affects land surface physical parameters and modulates the absorption and disposition of energy at land surface (Huang et al., 2020). For instance, LULCC induced changes in albedo, or the reflective properties of land surface, is highly relevant to the energy availability of the land surface (Burakowski et al., 2018; Jiang et al., 2021). Also, the characteristics of land surface hydrology and vegetation transpiration could further redistribute energy received by the surface (Alkama and Cescatti, 2016; Huang et al., 2020; Perugini et al., 2017).

In recent decades, the anthropogenically driven LULCC has dramatically altered the land cover patterns, with significant feedback

\* Corresponding author.

E-mail address: [lenggy@igsnrr.ac.cn](mailto:lenggy@igsnrr.ac.cn) (G. Leng).

to regional and global climate. At the same time, land management activities such as irrigation, fertilization and harvest also play a significant role in regulating the climate effect induced by LULCC. Although humans have investigated land cover change in approximately 18–29% of ice-free land, a much larger of the Earth's surface (42–58%) has not experienced land cover change but managed intensively to satisfy human demands for food (Luyssaert et al., 2014). There are numerous studies indicating the important effects of specific aspects of anthropogenically driven land use and land cover change. For instance, the cooling trends induced by irrigated area expansion have largely offset the warming trend due to greenhouse gas increases (Puma and Cook, 2010; Li et al., 2020b). Moreover, agricultural practices are able to mitigate heat extremes via enhanced evapotranspiration (Thiery et al., 2017; Mueller et al., 2016). In addition to irrigation, the increasing application of fertilization has greatly contributed to climate warming through enhanced emission of nitrous oxide ( $\text{N}_2\text{O}$ ) and methane ( $\text{CH}_4$ ) in agricultural land (Guardia et al., 2019). Globally, anthropogenic sources of  $\text{N}_2\text{O}$  and  $\text{CH}_4$ , which are dominated by agriculture, have increased by ~17% from 1990 to 2005 (Forster et al., 2007). Pugh et al. (2015) found that when land activities such as harvesting, grazing and tillage were considered in climate model, the land-use induced cumulative carbon losses were 70% greater than in simulations that ignored such processes. Recent studies suggested that increase in crop production during the 20th century accounts for about 25% of the observed increase in the amplitude of  $\text{CO}_2$  annual cycle (Gray et al., 2014; Zeng et al., 2014). Changes in forested land such as trees for wood products or fuel is also significant and has substantial carbon cycle consequences (Zubizarreta-Gerendaiain et al., 2016). Luyssaert et al. (2010) reported that the carbon flux due to wood harvest amounts to 15% of the forest net primary production in strongly managed regions such as Europe.

In short, changes in land use and land cover have greatly altered land surface water, energy and carbon fluxes (Alkama and Cescatti, 2016; Betts, 2000; Lee et al. 2011; Luyssaert et al., 2014; Zeng et al., 2017). In turn, these changes can modify air temperature ( $T_a$ ) locally and regionally through atmospheric circulation changes and teleconnection mechanisms (Li et al., 2020a; Wang et al., 2021). Many previous studies have investigated the climate effects of single land use or land management change such as global deforestation (Graesser et al., 2015; Perugini et al., 2017), vegetation greening (Li et al., 2020a; Zeng et al., 2017; Myers-Smith, 2020) or crop cultivation changes (Wang et al., 2021). However, the relative contribution of each type of land state-changes, land transitions and land managements to their climate effects remain underexamined. It is thus important to quantify the individual contribution of land state-changes, land transitions and land management to LULCC's climate effects, which is critical to enhancing our understanding of LULCC's role in global climate change.

To fill the gap, we aim to assess the effects of historical LULCC on global near-surface air temperature (except for Antarctic) and quantify the relative contributions of different types of land state-changes, land transitions and land management during 1901 to 2014, based on the latest Land-use harmonization version 2 dataset ( $0.25^\circ \times 0.25^\circ$ ). Specifically, the following scientific questions are addressed in this study: (1) How LULCC has influenced global temperature via biophysical mechanisms during 1901 to 2014? (2) which types of land-state change, land transition and land management dominate LULCC's temperature effect? Specifically, the latest CMIP6 climate models are used which allow for diagnosing the major physical processes governing LULCC's biophysical climate effect. The novelty of our study lies in explicitly assessing the relative contribution of different types of LULCC, and identifying which types of LULCC are most uncertain in climate models, thus guiding future model development efforts.

## 2. Materials and methods

### 2.1. Model simulations

In this study, land state, land transition and land management are defined following Lawrence et al. (2016). Specifically, land state indicates the characters of the Earth's surface and subsurface, which includes vegetation, soil, surface water, groundwater, biota, and human buildings etc. In the land model, they are generally represented by forested land, crop land, meadow or urban land. Land transition refers to the human-driven changes in land state. For example, a forested land may be left in its natural state, deforested, or used as urban land for human living. Land management refers to the manner humans handle vegetation, soil and water, including utilization of fertilizers and pesticides, selection of crop type, irrigation, or wood harvesting.

To quantify the temperature effect of LULCC, we used model simulations provided by the Land-Use Model Intercomparison Project (LUMIP), which is a part of the CMIP6 (the Sixth Phase of the Coupled Model Intercomparison Project models) (Lawrence et al., 2016). In LUMIP, control and sensitivity experiments are conducted for each participating climate model. For the control experiment, climate models are driven with historical variations of LULCC (hereafter referred to as “*land-hist*”). For this experiment, the spatial-temporal dynamics of historical land state, land transition, and land management are considered as in the CMIP6 historical simulation with all applicable land-use feature active (Lawrence et al., 2016). The sensitivity experiment (hereafter referred to as “*land-noLu*”) is the same as “*land-hist*”, but with all land state, transition and management (irrigation, fertilization, wood harvest and biofuel cultivation) maintained at the 1850 levels (Lawrence et al., 2016). Therefore, comparing the simulations between *land-hist* and *land-noLu* experiments could allow for quantifying the biophysical climate effects of LULCC, and analysing the associated changes in land surface energy, water and carbon fluxes induced by LULCC. After checking, only CESM2 and UKESM1-0-LL have provided simulations under *land-hist* and *land-noLu*. Therefore, simulations of the two models under *land-hist* and *land-noLu* are obtained for our analysis. Detailed information on the simulated variables used in our study is provided in Table S1 of supplementary. The model simulations can be downloaded from <https://esgf-node.llnl.gov/projects/cmip6/>.

### 2.2. Climate effect induced by LULCC

In this study, we focus on LULCC's biophysical climate effect on near-surface air temperature ( $\Delta T_a$ ), which can be calculated by the differences between the 2-m air temperature under “*land-hist*” ( $T2m_{land-hist}$ ) and that under “*land-noLu*” ( $T2m_{land-noLu}$ ). The calculation formula as follows:

$$\Delta T_a = T2m_{land-hist} - T2m_{land-noLu} \quad (1)$$

### 2.3. Land-use harmonization version 2

The Land-use harmonization version 2 (LUH2) is a new set of global gridded land-use forcing data set, which has been developed to characterize historical land-use and future projections in a standard format required by global climate models. Compared to CMIP5 land use maps, the LUH2 contains several new features with updated inputs, higher spatial resolution, as well as more detailed description of land-use transitions and agricultural management (Hurtt et al., 2011). The new data set includes annual land-use states, transitions and management layers for the years 850 to 2100 at a spatial resolution of  $0.25^\circ$  (<https://luh.umd.edu/data.shtml>). In this study, we used the LUH2 data set from 1901 to 2014 to assess the relative contribution of each type of land-state change, land transition and land management to LULCC's climate effect. Here, a total of 12 land state supplementary Table S2 and 113 land transitions are considered supplementary Table S3 and

Table S4. In addition, a total of 10 management activities including irrigation and fertilization are analysed across five cropland types (c3ann, c3per, c4ann, c4per and c3nfx) (supplementary Table S5). Since there are no changes in areas of biofuel crops in LUH2 from 1901 to 2014, the crpbf\_c3ann, crpbf\_c4ann, crpbf\_c3per, crpbf\_c4per, crpbf\_c3nfx are discarded in our analysis (supplementary Table S5).

#### 2.4. Ridge regression for weighting climate models

Since we have no observational data of  $\Delta T_a$  induced by LULCC, we have to assume that models showing better performance in estimating mean temperature are expected to have better ability of estimating  $\Delta T_a$ . Previous studies usually assigned equal weights to each climate model, based on which the ensemble mean is used for analysis. Here, we used different weights for the 2 climate models based on ridge regression (RR). In detail, the simulated temperature (under *land-hist*) from two climate model are regressed to observed temperature, based on which a linear regression model is fit and different weights for CESM2 and UKESM1–0–LL are obtained based on its regression coefficient. Compared to equal weighting, our approach generates an ensemble mean of temperature time series that has higher accuracy (supplementary Table S6). The regression coefficients and weights of the two models are presented in supplementary Table S7. The observed temperature is from Climatic Research Unit gridded time series (CRU) data set. The introduction of CRU data set can be found in supplementary Text S1. More details on RR and the training process can be seen in supplementary Text S2 and Text S3, respectively.

#### 2.5. Ridge regression for evaluating the relative contribution

Besides, RR is used to establish statistical relationship between changes in land state, land transition, land management and their climate effects to quantify the relative contribution (RC) of them. For RC of land state change and land management, we established the regression model between LULCC's temperature effect ( $\Delta T_a$ ) and 12 land state changes and 2 land managements (irrigation and fertilization) during 1901 to 2014, based on which the relative contribution of each land state change and land management is estimated via regression coefficient. The calculation principle of RC is presented in next paragraph. The statistical relationship is described as follows:

$$\Delta T_a \leftarrow A_{c3ann} + A_{c3per} + A_{pastr} + A_{c3nfx} + A_{c4per} + A_{urban} + A_{range} + A_{secdf} + A_{c4ann} + A_{primf} + A_{primm} + A_{secdn} + A_{irr} + R_{fer} \quad (2)$$

Where A represents the area of each land state and irrigation area during 1901 to 2014; R represents the total nitrogen fertilizer rate for all types of crops. The land state includes: C3 annual crops (c3ann); C3 perennial crops (c3per); managed pasture (pastr); C3 nitrogen-fixing crops (c3nfx); C4 perennial crops (c4per); urban land (urban); range-land (range); potentially forested secondary land (secdf); C4 annual crops (c4ann); forested primary land (primf); non-forested primary land (primm); Potentially non-forested secondary land (secdn).

The RR model enables us to estimate the regression coefficients (REC) for each explanatory variable. Generally, higher regression coefficients have larger impacts on the regression results (dependant variable). The relative contribution of each explanatory variable is calculated by the standardized ratio of  $\frac{|REC_{EV}|}{\sum |REC_{EV}|} \times 100\%$ . The RC of all the variables thus represent the percentages and possess a property by which they sum to 100%. The above calculating methods based on regression coefficient have been widely used to evaluate the relative contribution (or weight or relative importance) in many studies such as Dul et al. (2011), Doetterl et al. (2015), Rasmussen et al. (2018) and Oster (2019).

Further, we calculated the corresponding temperature change (CTC) induced by changes in each land state and land management based on

RC:

$$CTC = RC \times \Delta T_a \quad (3)$$

The derived CTC of each land state area change and the associated land transition areas are used to establish statistical regression model to quantify the RC of each land transition. Taking pastr as an example, the statistical relationship is as below:

$$CTC_{pastr} \leftarrow LTA_{c3ann} + LTA_{c3nfx} + LTA_{c3per} + LTA_{c4ann} + LTA_{c4per} + LTA_{range} + LTA_{secdf} + LTA_{secdn} + LTA_{urban} \quad (4)$$

Where  $CTC_{pastr}$  is the temperature changes induced by pastr change, which is calculated by the Eq. (3); the right hand of Eq. (4) indicates the area transitioned from pastr to c3ann, c3nfx, c3per, c4ann, c4per, range, secdf, secdn and urban, respectively. LTA is the land transition area between land use states.

Similarly, we quantified the relative contribution of five croplands (including c3ann, c3per, c4ann, c4per, c3nfx), regarding their expansion of irrigated area (IA) and application of nitrogen fertilizer (ANF). The statistical relationship as below:

$$CTC_{irr} \leftarrow IA_{c3ann} + IA_{c3per} + IA_{c4ann} + IA_{c4per} + IA_{c3nfx} \quad (5)$$

$$CTC_{fer} \leftarrow ANF_{c3ann} + ANF_{c3per} + ANF_{c4ann} + ANF_{c4per} + ANF_{c3nfx} \quad (6)$$

## 3. Results

### 3.1. Temporal changes in LULCC's impact on temperature

The temporal changes of annual and seasonal climate effect ( $\Delta T_a$ ) induced by LULCC are presented in Fig. 1. Both CESM2 and UKESM1–0–LL simulate an upward trend in  $\Delta T_a$  during 1901–2014 (Fig. 1a), suggesting that historical LULCC has exerted a warming trend for the globe as a whole. However, large differences are found between the two models. For example, CESM2 simulates an increasing trend of  $\Delta T_a$  at a rate of 0.0039 °C/century, which more than doubles that by UKESM1–0–LL (0.00188 °C/century) (Fig. 1a). In addition, positive values of  $\Delta T_a$  are simulated by UKESM1–0–LL during the whole study period, while negative  $\Delta T_a$  is found for CESM2 before 1960s (Fig. 1a). Seasonally, UKESM1–0–LL shows a positive  $\Delta T_a$ , induced by LULCC for all seasons, with the highest warming trend in winter (0.00287 °C/century) and lowest warming trend in spring (0.00141 °C/century) (Fig. 1b–1e). In contrast, CESM2 simulates a cooling effect during the whole period in spring (Fig. 1b), exhibiting a non-significant change trend in  $\Delta T_a$ . In autumn, though both models agree with the sign of  $\Delta T_a$ , the change trend in CESM2 is four times larger than that in UKESM1–0–LL.

The revealed large discrepancies between CESM2 and UKESM1–0–LL point to the importance for weighting the two models for our following analysis. Based on the weighted mean of the two models, we found that global LULCC has caused a significant warming effect during the past 114 years, at a rate of 0.0025 °C/century (Fig. 1a). Seasonally, the largest warming effect of LULCC occurs in autumn, with  $\Delta T_a$  ranging from 0.0004 °C/year to 0.005 °C/year (Fig. 1d). In addition, the largest warming trend is found in autumn ( $3.62 \times 10^{-3}$  °C/century) followed by winter ( $3.38 \times 10^{-3}$  °C/century), summer ( $1.92 \times 10^{-3}$  °C/century) and spring ( $1.10 \times 10^{-3}$  °C/century) (Fig. 1b–1e).

### 3.2. Spatial pattern of LULCC's impact on temperature

Spatial patterns of the long-term mean of  $\Delta T_a$  are shown in Fig. 2–3. For CESM2, LULCC exerts a cooling effect on average in the Northern Hemisphere, mainly due to strong cooling signals in the U.S., central Asia and eastern Europe. In contrast, a strong warming effect of LULCC is found from 20°N to 40°S especially in Brazil, western Africa and southeast Asia (Fig. 2a). For UKESM1–0–LL,  $T_a$  changes more in warm regions than in cold regions, mainly concentrated from 60°N to 40°S

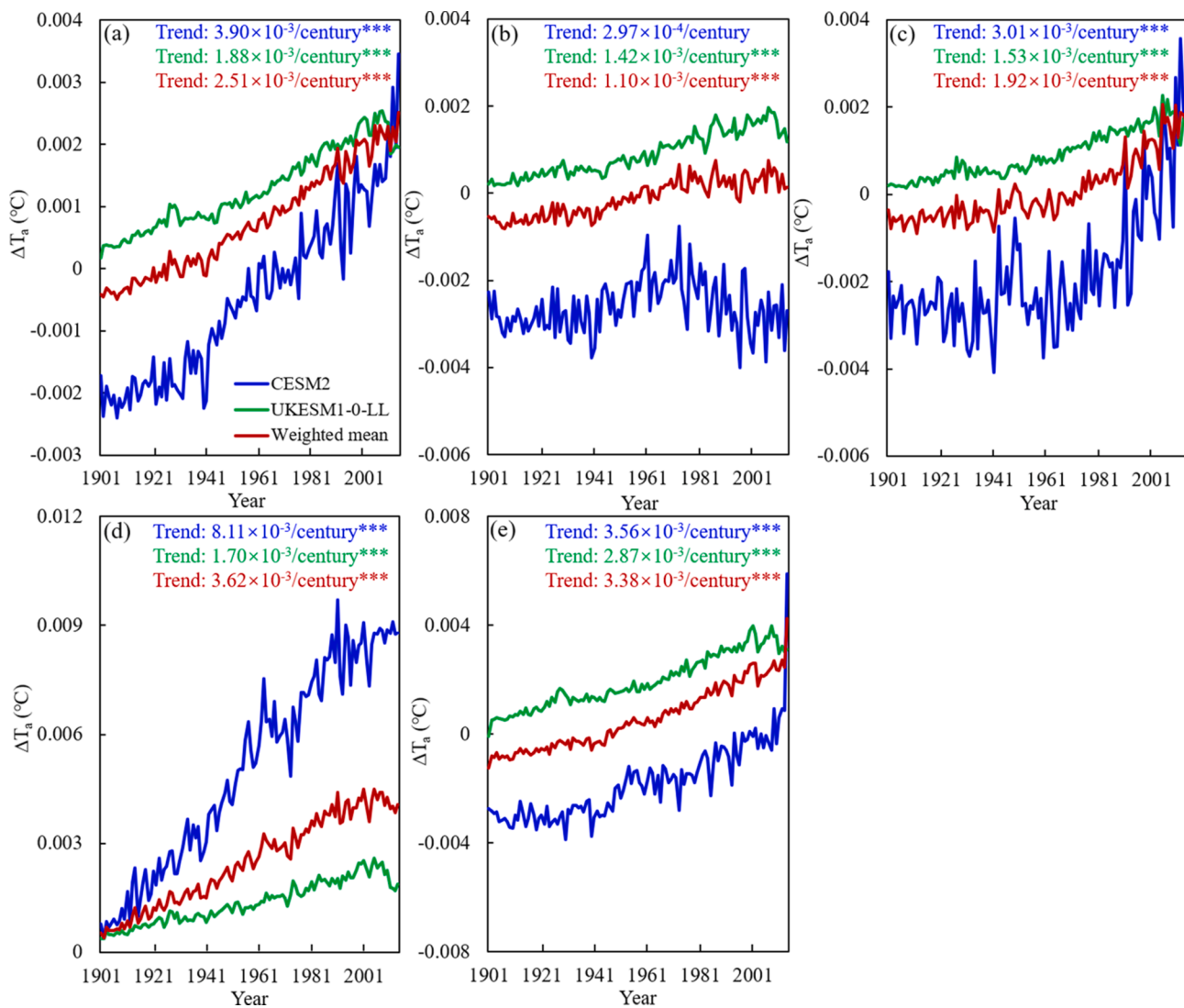


**Fig. 1.** Near-surface air temperature changes ( $\Delta T_a$ ) induced by land use and land cover change (LULCC) over global land areas based on CESM2, UKESM1-0-LL and weighted mean of two models. (a) is the annual  $\Delta T_a$ , (b)-(e) indicate the seasonal  $\Delta T_a$  (a: spring, b: summer, c: autumn, d: winter). \*\*\* indicates the statistical significance at 0.1% level.

(Fig. 2b). Generally, the weighted mean of  $\Delta T_a$  shows a similar spatial pattern to that of CESM2, though it has lower  $\Delta T_a$  (Fig. 2c). At the seasonal scale, CESM2 simulates a large cooling effect in areas between 60°N to 20°N during spring, summer and winter, while a warming effect is found in Brazil, tropical rainforest areas in Africa and southeast Asia (Fig. 3a, 3d and 3j). In autumn, CESM2 suggests that LULCC has exerted a warming effect in most of the global land areas (Fig. 3g). Compared to CESM2, the UKESM1-0-LL show a lower climate effect induced by LULCC ( $\Delta T_a$ : -0.1 ~ 0.1 °C), with a opposite signal (cooling effect) found in the Northern Hemisphere during spring, summer and winter (Fig. 3b, 3e and 3k). Based on the weighted mean, the spatial patterns of climate effect induced by LULCC is similar to that of CESM2 at four seasons, with a relatively smaller  $\Delta T_a$  range at global scale (Fig. 3c, 3f, 3i and 3l).

In this study, we also carried out a briefly analysis about the  $\Delta T_a$  at different climate regions, based on the map of IPCC-WGI reference climate regions (Iturbide et al., 2020). Particularly, some geographically similar climatic regions are merged, resulting in 14 climatic regions (Fig. 4). Overall, the LULCC generates relatively large cooling effect in SNA, Eur, and NA at annual scale, with  $\Delta T_a$  ranging from -0.00016 to -0.0056 °C/yr (Fig. 4d-4f). Oppositely, a great warming effect of LULCC is found in the climate region of CNA, CAS, NSA, SSA, CSA and SEA with

$\Delta T_a$  ranging from 0.00508 to 0.131 °C/yr (Fig. 4g, 4i, 4j, 4k and 4m). Seasonally, a large cooling effect is found in the climate regions of SNA, Eur and NA ( $\Delta T_a$  from -0.00196 to -0.017 °C/yr) in Spring, Summer and Winter (Fig. 4d-4f), while a warming effect is found across SEA, SSA, NSA and CSA (Fig. 4i-4k and 4 m). During autumn, LULCC have a warming effect in most climate regions except for Aust (-0.00157 °C/yr), NA (-0.00045 °C/yr) and GL ( $-2.35 \times 10^{-5}$  °C/yr) (Fig. 4b, 4e and 4n). By dividing the study period to two equal sub-periods (i.e., 1901–1957 and 1958–2014), we found a larger temperature effect of LULCC in recent decades (1958–2014), particular in SEA, CAN, NSA, SSA and CSA climate regions (Fig. S1). Similarly, at different seasons, the temperature effect of LULCC in the period of 1958–2014 is basically higher than that during 1901–1957 (Fig. S2-S5).

During the study period 1901–2014, the  $\Delta T_a$  has exhibited a significant decreasing trend between 60°N and 40°N based on CESM2, especially in northwest U.S., eastern Europe and India with a trend of -0.1 ~ -0.25 °C/century (Fig. 5a). Oppositely, an increasing trend in  $\Delta T_a$  mainly concentrates in Brazil, western Africa and southeast Asia at a rate of 0.1 ~ 0.48 °C/century (Fig. 5a). In contrast, a significant ( $p < 0.05$ ) increasing trend is found for most of global land areas based on UKESM1-0-LL (Fig. 5b), with the change rate ranging from -0.005 to 0.04 °C/century. Similar to CESM2, the anthropogenically driven

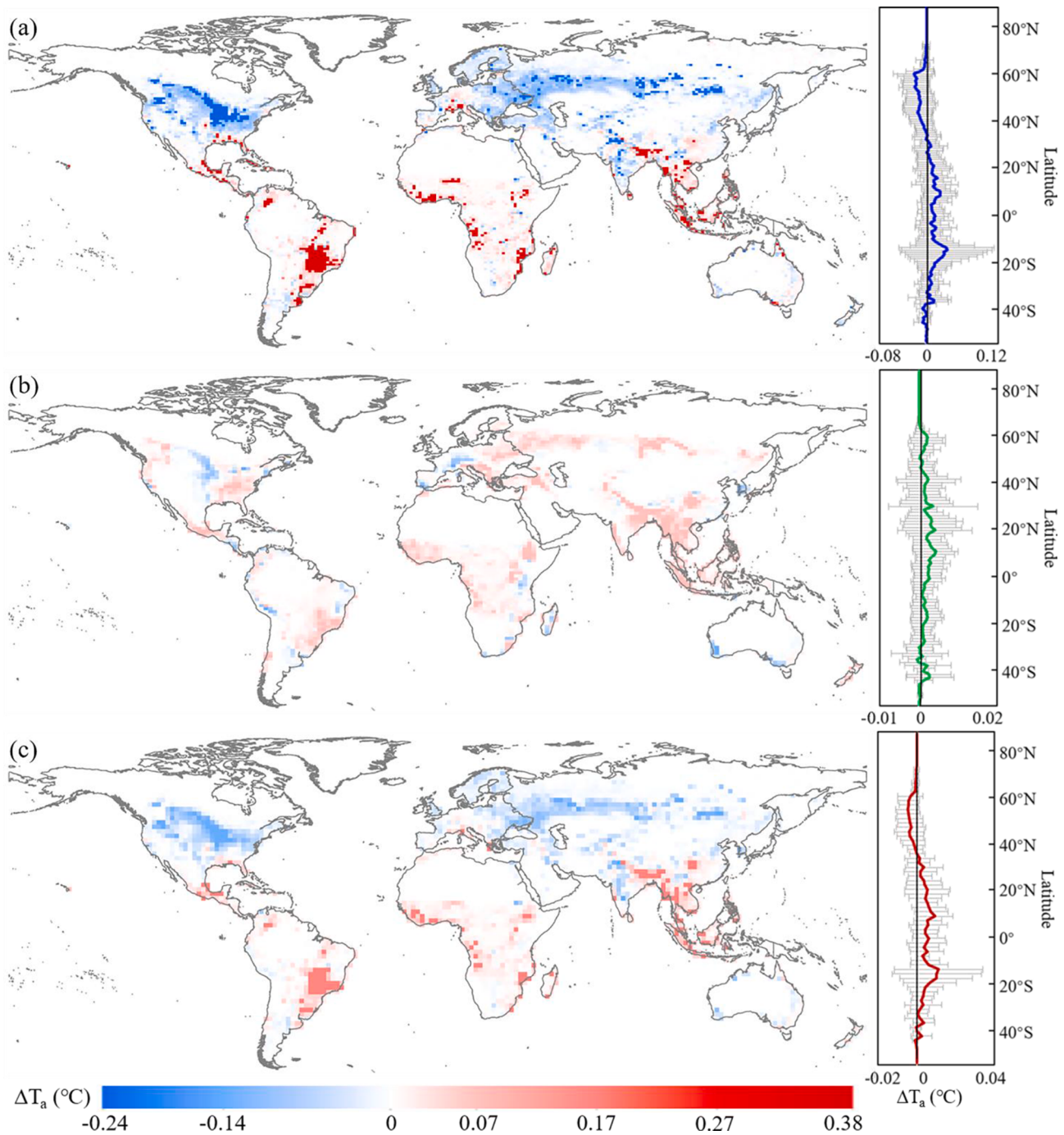


**Fig. 2.** The spatial patterns of annual temperature changes ( $\Delta T_a$ ) induced by LULCC based on CESM2 (a), UKESM1-0-LL (b) and weighted mean of two models (c) from 1901 to 2014. The line charts indicate the latitudinal distribution of  $\Delta T_a$ , and the grey bar represents the standard deviation of all  $\Delta T_a$  pixel values at the same latitude.(For interpretation of the references to colour in this figure legend, the reader is referred to the web version of this article.)

LULCC have significantly ( $p < 0.05$ ) decreased in areas from 60°N to 40°N except for central Europe according to weighted mean, while an upward trend is found from 40°N to 30°S (Fig. 5c). Seasonally, the cooling and warming trend induced by LULCC is concentrated in areas from 60°N to 40°N and from 40°N to 30°S in spring, summer and winter, respectively (Fig. 6). Particularly, a consistent upward trend of  $\Delta T_a$  is found from 60°N to 30°S in autumn (Fig. 6g-6i).

### 3.3. Relative contribution of different types of LULCC

In this study, we quantified the RC of each type of land state change, land transition and land management to the changes in  $\Delta T_a$  during 1901

to 2014. The RC of land state change and land management to  $\Delta T_a$  caused by LULCC is presented in Fig. 7. Although the same input (LUH2) is used for CESM2 and UKESM1-0-LL, a large divergence is found in the RC of different land state and land management. In CESM2, changes in secdn contribute the largest to  $\Delta T_a$ , with RC up to 20.20%, followed by c3per (15.79%), c4ann (13.60%), urban (10.07%), primn (9.69%), range (9.27%), pastr (7.16%), c4per (3.42%), primf (2.78%), secdf (2.48%), c3nfx (2.14%), irrigation (1.68%), c3ann (1.09%) and fertilization (0.62%) (Fig. 7a). However, for UKESM1-0-LL, the largest contribution is from changes in c3ann, primf, c3nfx, c3per and c4per, with total RC above 60% (Fig. 7b). The weighted mean of CESM2 and UKESM1-0-LL exhibits smaller RC range for different land state and land

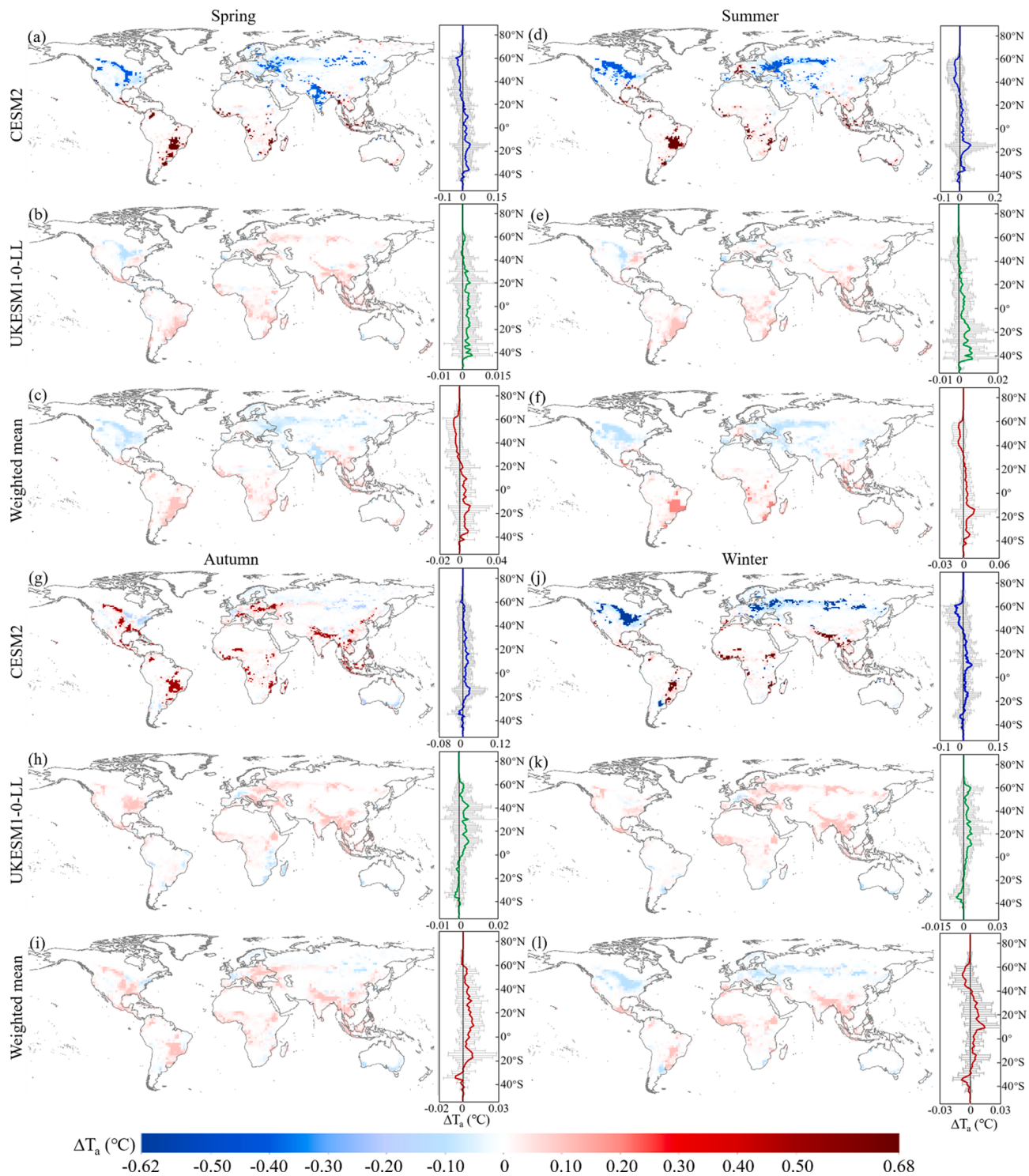


**Fig. 3.** The spatial patterns of seasonal temperature changes ( $\Delta T_a$ ) induced by LULCC from 1901 to 2014. (a-c): spring, (d-f): summer, (g-i): autumn, (j-l): winter. The line charts indicate the latitudinal distribution of  $\Delta T_a$ , and the grey bar represents the standard deviation of all  $\Delta T_a$  pixel values at the same latitude. (For interpretation of the references to colour in this figure legend, the reader is referred to the web version of this article.)

management, with RC ranging from 3.84% to 9.60% (Fig. 7c). Particularly, land management (irrigation and fertilization) has contributed the largest to  $\Delta T_a$  changes, with RC up to 18.41% (Fig. 7c).

Fig. 8 shows the RC of each land transition and crop management to  $\Delta T_a$ . For CESM2, the greatest contribution to  $\Delta T_a$  is made by decreases in secdn, which is replaced by urban (22.28%), c4per (21.02%) and c3per (18.9%) (Fig. 8k). The substitution of c3per by secdf, urban and secdn is also a major driver of LULCC-induced air temperature change,

with total RC above 90% (Fig. 8c). For UKESM1-0-LL, the land transition between different cropland types has resulted in a large impact on  $\Delta T_a$  changes. Specifically, the c3ann transition to c3nfx contributed about 53% of  $\Delta T_a$  change, while the transition of c3nfx to c4ann contributed about 53.9% (Fig. 8a and 8h). In addition, the replacement of secdn by c3per, c3nfx and c4ann also largely contribute to  $\Delta T_a$  in UKESM1-0-LL, with total RC of 76.4% (Fig. 8k). Based on the weighted mean, the replacement of secdn by cropland has the greatest

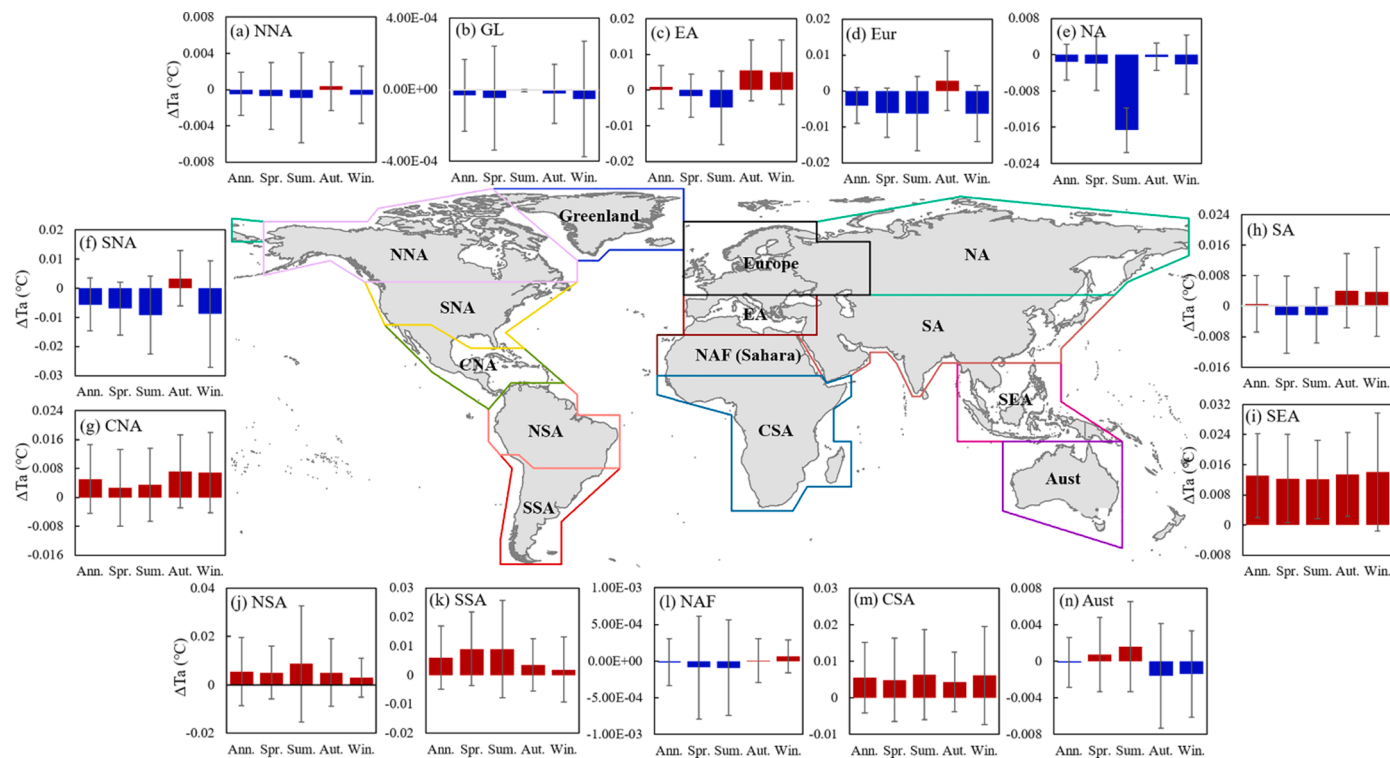


**Fig. 4.** The comparison of annual and seasonal temperature effect of LULCC at different climate region during 1901 to 2014. The error bar is the standard deviation of all pixel value in same climate region; the blue bar represents the cooling effect of LULCC; the red bar indicates the warming effect of LULCC; Ann: annual; Spr: spring; Sum: summer; Win: winter. NNA: northern North-America; SNA: southern North-America; CAN: central North-America; NSA: northern South-America; SSA: southern South-America; NA: northern Asia; SA: southern Asia; EA: parts of Europe and Africa; NAF: northern Africa; CSA: central and southern Africa; SEA: southeast Asia; Aust: Australia; GL: Greenland; Eur: Europe. (For interpretation of the references to colour in this figure legend, the reader is referred to the web version of this article.)

contribution to  $\Delta T_a$  (Fig. 8k). Besides, the transition of original land state to cultivation land (such as c3ann, c4ann, c3nfx and c3per), grazing land (such as range and pastr) or urban land has a large contribution to climate effect (Fig. 8). Notably, it can be found that there is a great difference between the two models (CESM2 and UKESM1–0–LL) in representing the climate effect of different types of cropland transitions (Fig. 8a–8d, 8 h).

The RC of each type of cropland management to climate effect is presented in Fig. 8m and 8n. Overall, the climate effect of irrigation is larger than that of nitrogen fertilizer application (Fig. 7). Particularly, the application of nitrogen fertilizer in C3 plant has larger contribution compared to C4 plants (Fig. 8m). In addition, irrigation has almost the same contribution for different types of croplands (Fig. 8n).

#### 4. Discussions

This study shows that LULCC is an important driving factor for global climate change based on the latest LUMIP, although its effect is far below that by greenhouse gases emissions. We found that LULCC has a small biophysical temperature effect ( $-0.0005 \sim +0.0023^{\circ}\text{C}/114$  years) on global climate based on weighted mean of two climate models. Generally, a cooling effect of LULCC is found between  $60^{\circ}\text{N}$  and  $40^{\circ}\text{N}$  based on weighted mean, particularly in the U.S, eastern Europe, central Asia (Fig. 2). For the above regions (the U.S, eastern Europe, central Asia), a significant ( $p < 0.05$ ) increase in potentially forested secondary land (secdf) and rangeland is found (Fig. S6i and S6j), which would give rise to higher evaporation and thus generate cooling effect (Shen et al., 2015; Tan et al., 2018). Moreover, vegetation photosynthesis is able to absorb large amount of  $\text{CO}_2$  and contribute to cooling effect for local environment (Lucht et al., 2002; Shen et al., 2015).

Oppositely, a significant increasing warming trend is detected in

Brazil, central Africa and southeast Asia associated with intensive deforestation (Fig. S6g and S6h). Deforestation exerts a warming impact on climate by (i) releasing more  $\text{CO}_2$  to the atmosphere, (ii) eliminating the potential increase of carbon storage in trees due to future  $\text{CO}_2$  fertilization, and (iii) reducing evapotranspiration especially in the tropics (Jiang et al., 2021; Scott et al., 2018; Winckler et al., 2019; Zemp et al., 2017). In addition to deforestation, other land activities (such as cultivation, livestock production, fertilization and irrigation, etc.) have greatly influenced global climate (Leip et al., 2015; Wang et al., 2021). Because they are capable of generating greenhouse gas emission by sources and removals by sinks, followed by loss from decomposition and fire, including complex microbial process associated with human management and ecosystems disturbance (Ghimire et al., 2017; Jose et al., 2016; Xia et al., 2022). Consequently, policymakers have to explicitly consider the climate effects of each land activities before formulating land use plans. What's more, temperature changes induced by LULCC do have large spatial variability and have teleconnections with climates in other regions of the globe. For instance, the warming effects in high altitude regions (such as the Tibetan Plateau) is likely to result in release of greenhouse gas from thawing permafrost (Schuur et al., 2015; Yang et al., 2010; Zona, 2016), while a strong cooling effect in Nepal and north India may protect permafrost from thawing. Accordingly, the climate effects of LULCC not only directly alter global temperature, but also have secondary impacts on natural greenhouse gas fluxes through biogeochemical cycles, which should be also taken into account when carrying out large-scale land activities in the future. At the same time, the altered atmospheric circulation is also a major contributor to the net change in global air temperature (Horton et al., 2015), but its spatial variations may depend on the selection of the climate model, and related uncertainties require to be further investigated.

Indeed, LULCC alters global climate via both biogeochemical and

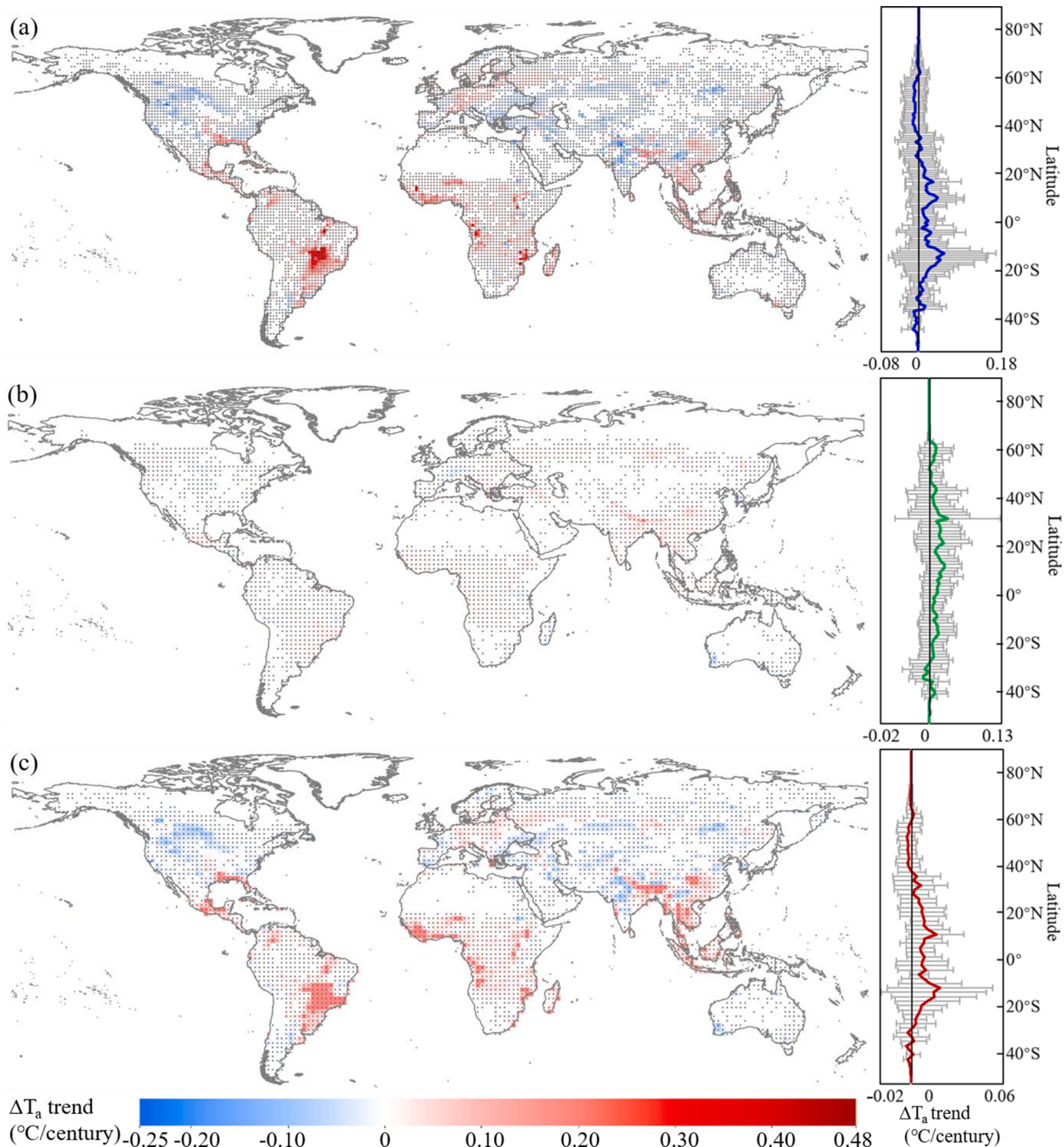


**Fig. 5.** The spatial patterns of change trend in LULCC's temperature effect ( $\Delta T_a$ ) based on CESM2 (a), UKESM1–0–LL (b) and weighted mean of two models (c) during 1901 to 2014. The line charts indicate the latitudinal distribution of  $\Delta T_a$  trend simulated by CESM2 (d), UKESM1–0–LL (e) and weighted mean of two models (f). The grey bar represents the standard deviation of all  $\Delta T_a$  trend pixel values at the same latitude. Black point in a–c indicates grid cells with significant ( $p < 0.05$ ) change trend. (For interpretation of the references to colour in this figure legend, the reader is referred to the web version of this article.)

biophysical processes. Although this study focuses on the biophysical temperature effect induced by LULCC, the coupling temperature effect deserves to be explored. We therefore compared the coupling temperature differences between two scenarios (historical and land-hist) for CESM2 and UKESM1–0–LL (Fig. S7 and S8), and found that: 1) the coupling temperature effect of LULCC shows great temporal fluctuation and spatial difference, which is closely related to the type and intensity

of land activities carried out by humans in different periods and regions; 2) The coupling temperature effect of LULCC is much larger than the biophysical temperature effects alone, which indicates that the biogeochemical process induced by LULCC is the dominant factor affecting the global climate; 3) Although the LUMIP use the same data inputs (LUH2), earth system models have large uncertainties in simulating the temperature effects of LULCC. As the simulations of carbon and nitrogen flux

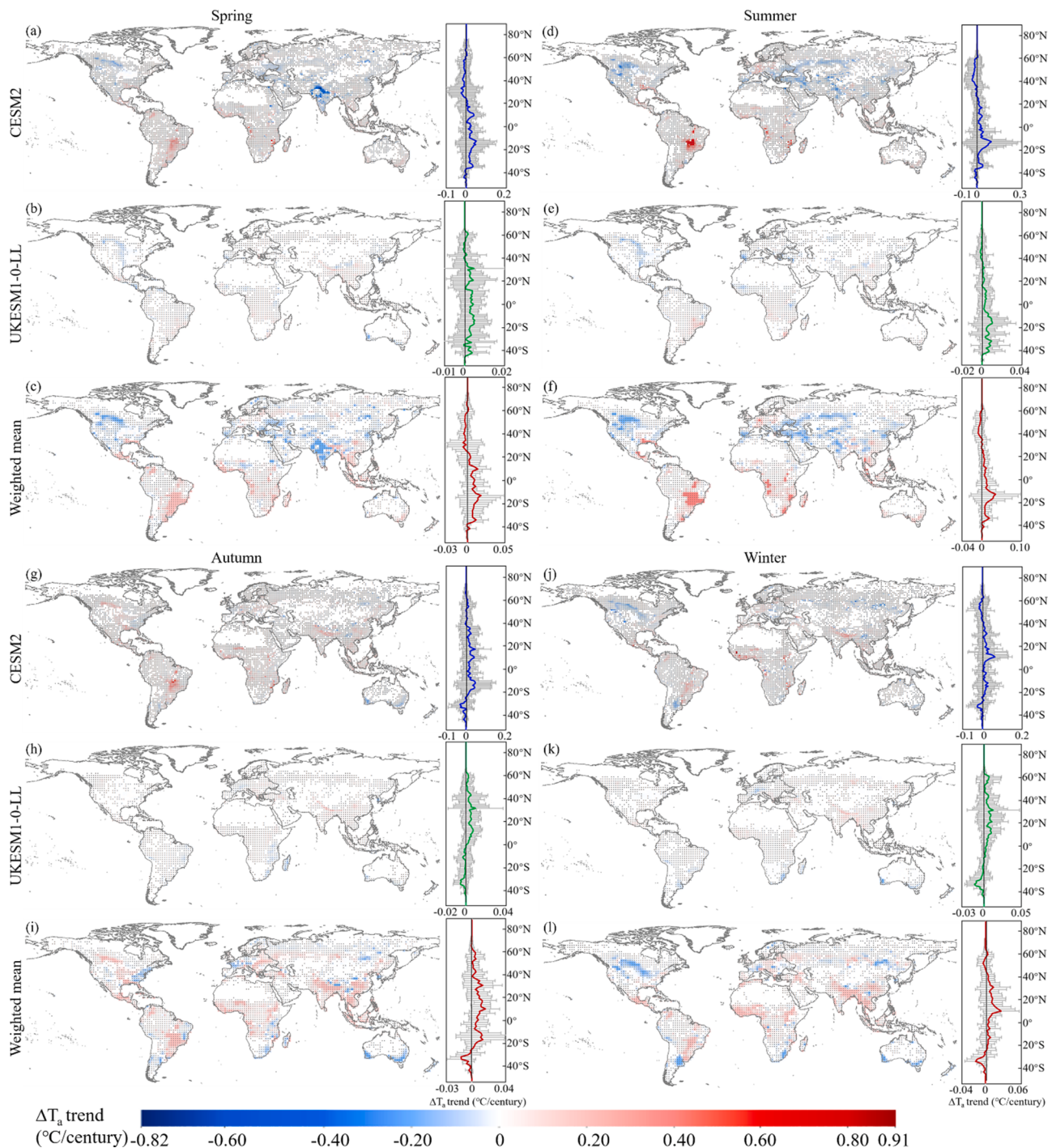


**Fig. 6.** The spatial patterns of change trend in LULCC's temperature effect ( $\Delta T_a$ ) based on CESM2, UKESM1-0-LL and weighted mean of two models at different seasons during 1901 to 2014. The line charts indicate the latitudinal distribution of  $\Delta T_a$  trend. The grey bar represents the standard deviation of all  $\Delta T_a$  trend pixel values at the same latitude. Black point in a-c indicates grid cells with significant ( $p < 0.05$ ) change trend. The (a-c): spring; (d-f): summer; (g-i): autumn; (j-l): winter. (For interpretation of the references to colour in this figure legend, the reader is referred to the web version of this article.)

are not provided in LUMIP, further decomposition of LULCC's impact on biogeochemical processes is not conducted in this study.

Here, we further estimated the contribution of each energy flux to climate effect based on land surface energy balance, which is greatly helpful to understand the process of biophysical-based climate effect due to LULCC (Fig. S9-S11). The calculation processes are shown in supplementary Text S4. Overall, LULCC leads to an increase in albedo, with subsequent cooling effect on global climate during the past 114 years especially in the eastern U.S., Brazil and southeast Asia due to decrease

in forested land (Fig. S9 and S10). Generally, forested landscape is darker due to lower albedo than open land, particularly in high latitude regions during seasons with snow cover (Perugini et al., 2017; Yu and Leng, 2022; Yu et al., 2022). Therefore, deforestation, with few exceptions, result in higher albedo and less net radiation at the land surface, with a potential decrease of land surface temperature (Perugini et al., 2017; Zhai et al., 2014). Besides, our findings suggest that the aerodynamic resistance ( $r_a$ ) is a dominant factor in controlling biophysical warming effects of LULCC, and its effects have increased significantly

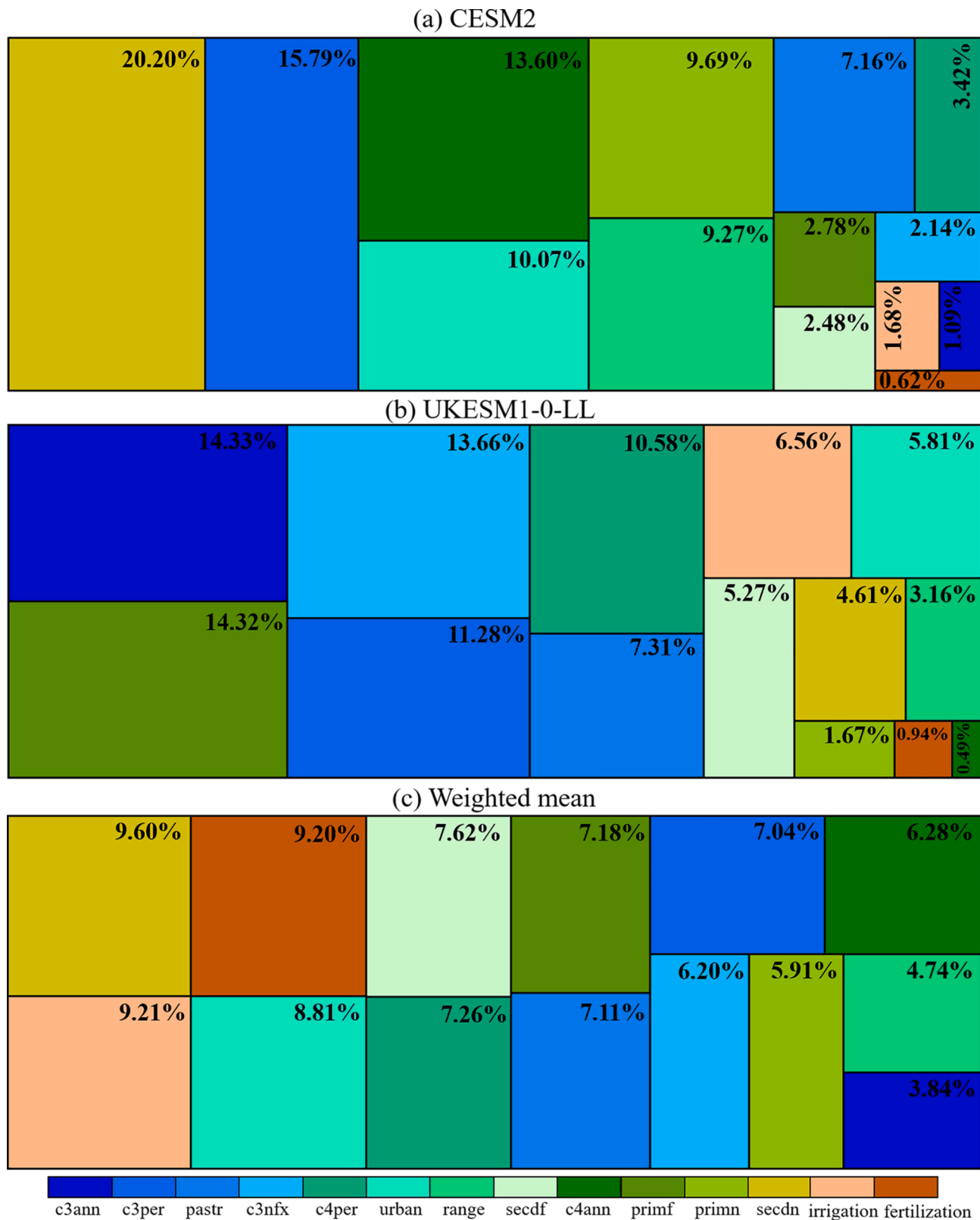


**Fig. 7.** The relative contribution (RC) of land state change and land management (irrigation and fertilization) to LULCC's temperature effect based on CESM2, UKESM1-0-LL and weighted mean of two models (c) at global land during 1901 to 2014. primf: forested primary land; primn: non-forested primary land; secdf: Potentially forested secondary land; secdn: Potentially non-forested secondary land; pastr: managed pasture; range: rangeland; urban: urban land; c3ann: C3 annual crops; c3per: C3 perennial crops; c4ann: C4 annual crops; c4per: C4 perennial crops; c3nfx: C3 nitrogen-fixing crops.

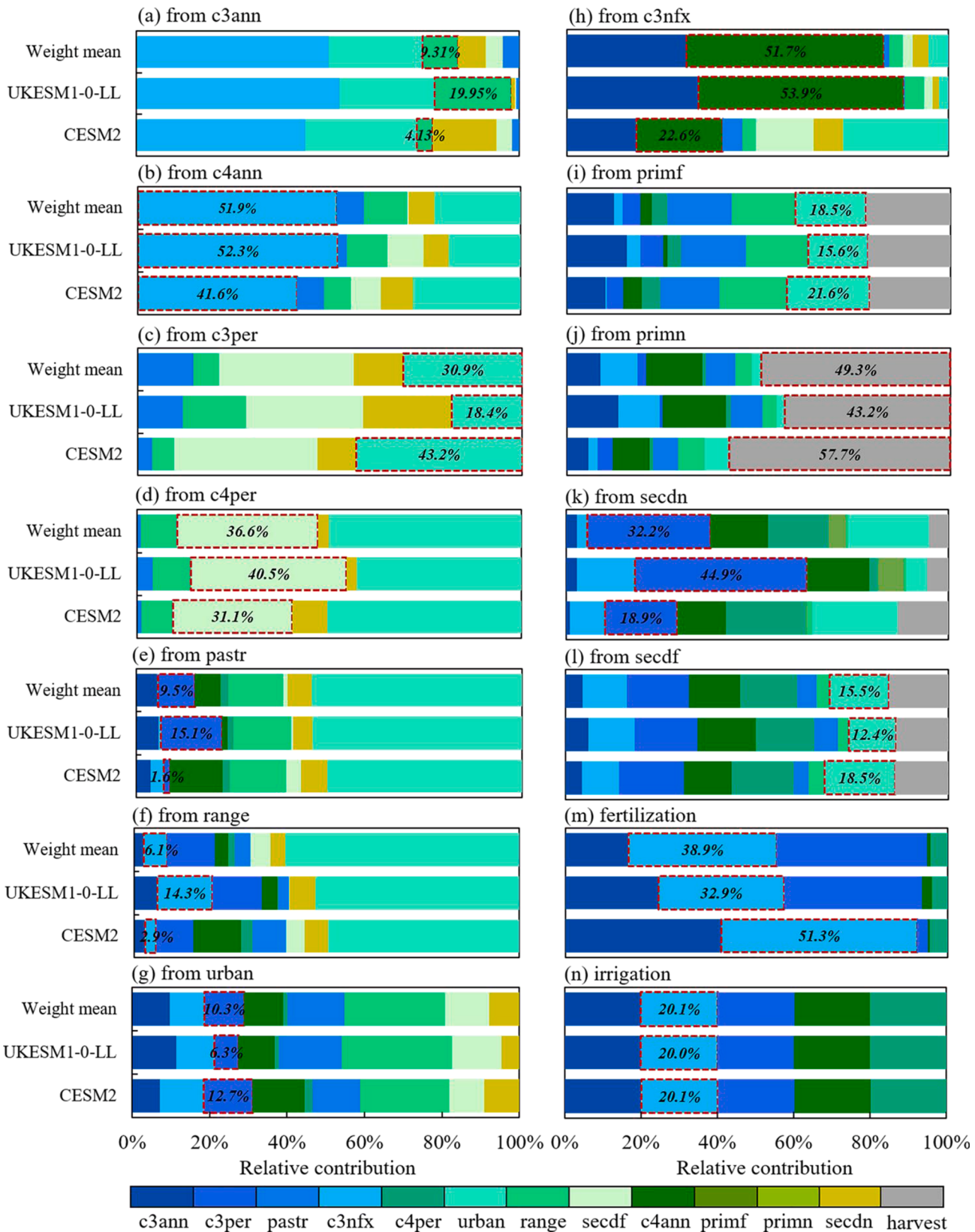


**Fig. 8.** The relative contribution (RC) of land transition (a-l) and land management (m and n) to LULCC's temperature effect based on CESM2, UKESM1-0-LL and weighted mean of two models at global land during 1901 to 2014. The red box indicates the type of land transition, which have the largest differences in RC between CESM2 and UKESM1-0-LL.

over time (Fig. S9). In recent decades, the intensive anthropogenically driven LULCC (mostly deforestation) has caused an increase of aerodynamic resistance, thereby limiting the turbulent heat transfer between land and atmosphere, especially latent heat flux (Liao et al., 2018, 2020). The decrease in latent heat flux thus contributes to global warming over time (Fig. S9). Previous studies have indicated that forest clearing may give rise to evaporative cooling during spring and summer period because crops generally have larger evaporation rates than forest if the water supply is sufficient especially in the temperate regions (Noblet-Ducoudré et al., 2012; Stoy, 2018).

This study demonstrates the great differences in climate effects of land transitions between land use states, due to the fact that surface or near-surface temperature varies largely depending on the land cover type (Boone et al., 2016; Tran et al., 2017; Trlica et al., 2017). Based on weighted mean, changes in forested/non-forested secondary land, urban land and cropland have contributed above 70% to LULCC induced temperature change (Fig. 7c). amongst the 113 types of land transitions, the land use types replaced by cropland dominate the climate effect induced by LULCC (Fig. 8). Globally, croplands, occupying approximately 13% of the land surface, play an important role in the climate system through biogeochemical and biophysical feedbacks to the atmosphere (Zhang et al., 2013; Zhou et al., 2021). Numerous studies indicated that the conversion of forested land to agricultural land is highly associated with climate change in specific regions (Chen and Dirmeyer, 2016; Graesser et al., 2015; Kala and Hirsch, 2020; Lee et al., 2011). Particularly, deforestation for agriculture has been mostly indicated as a heat source in the tropical regions and a heat sink in the boreal region (Chen and Dirmeyer, 2016; Lee et al., 2011; Zeng et al., 2021; Zhou et al., 2021). Besides, the wood harvest also has a relatively large contribution to climate effect, through regulating biophysical characteristics such as albedo, evapotranspiration, roughness and heat capacity, etc. (Zhou et al., 2021). For instance, the increase of aerodynamic resistance largely contributes to the warming effect in the U.S. and tropic zone (Fig. S10 and S11). On the other hand, rapid urbanization with increasing population makes urban regions a heat source due to increased greenhouse gas emission, reduced vegetated surface and increased anthropogenic waste heat (Huang et al., 2019)

The climate effect of land management (including fertilization and irrigation) on global climate are found during the study period. Generally, agricultural irrigation has greater contribution to temperature change at global scale compared to fertilization. Irrigation plays a critical role in sustaining crop production in water-limited regions, enhancing soil evaporation and crop transpiration with subsequent cooling effects (Li et al., 2020b; Yang et al., 2020). Besides, similar RC of irrigation is found for different types of crops (c3ann, c3nfx, c3per, c4per and c4ann), while the climate effect of fertilization is highly dependant on the crop types. The cultivated Nitrogen (N)-fixing crops (c3nfx) are able to mitigate climate warming, by relieving N limitation of plant growth which promotes carbon dioxide ( $\text{CO}_2$ ) sequestration in plant biomass (Good, 2018; Wang et al., 2018). This well explains the findings of our study that fertilizing c3nfx contribute the largest to temperature change. Therefore, the choice of crop types to grow in the future should take into account both their productivities and the climate effects.

Finally, the revealed uncertainty of LULCC's climate impact is substantial, as indicated by the large difference in the climate effects and RC between CESM2 and UKESM1–0–LL. First, the large divergence between the two models is due to the large diversity in their representation of LULCC. In fact, it is non-trivial to define the terms "land use", especially the term "sustained land use" (Lawrence et al., 2016). Although LUMIP has clarified the treatment of constant land use based on LUH2, there are differences in LUH2's application scheme, which contributes to the differences in the simulations (Lawrence et al., 2016). Second, different models have different sensitivity to LULCC and land management in various scenarios. Despite the uncertainty, LUMIP is still the most valuable project for assessing the impact of LULCC on global climate

system, and is unique for quantifying the individual effect of different types of LULCC.

## 5. Conclusions

Previous studies have well assessed the impacts of LULCC on global and regional climate, but with few attentions paid to the relative contribution of different types of LULCC. This study fills the gap by evaluating global temperature effect of LULCC based on CMIP6 during 1901 to 2014, with a focus on the relative contribution of 12 land state changes, 113 land transitions and 10 land managements. The main findings of this work are as follows:

- 1) There is a large divergence in the simulated LULCC's biophysical temperature effect between CESM2 and UKESM1–0–LL. Particularly, the two models even disagree with the sign of LULCC's impact on surface air temperature in the northern hemisphere except for autumn. Based on the weighted mean of the two models, we found a significant warming effect at a rate of 0.0025 °C/century, and the largest warming effect of LULCC occur in autumn. Spatially, LULCC's impact on temperature exhibited a significant ( $p < 0.05$ ) cooling trend ( $-0.01$  °C to  $-0.03$  °C) in areas from  $60^{\circ}\text{N}$  to  $40^{\circ}\text{N}$ , while a warming trend ( $+0.03$  °C to  $+0.11$  °C) is found from  $40^{\circ}\text{N}$  to  $30^{\circ}\text{S}$ .
- 2) Based on CESM2, the secdn change contributes the largest to the climate effect, with RC of 20.20%. However, ULES1–0–LL suggests that the largest contribution to climate effect is caused by changes in cropland and forested primary land (c3ann, primf, c3nfx, c3per and c4per), with total RC above 60%. After weighting the two models, a smaller RC range is obtained for different land state and land management, with RC ranging from 3.84% to 9.60%. In addition, irrigation and fertilization have greatly contributed to LULCC's climate effect, with RC up to 18.41%. Overall, the large difference in temperature effect between CESM2 and UKESM1–0–LL is due to their difference in simulating the forestland and cropland changes.
- 3) CESM2 suggests that the largest contribution to LULCC's climate effect is caused by decreased secondary forested land, which is mainly replaced by urban land (22.28%), cropland (c4per and c3per) (39.92%). For UKESM1–0–LL, the transition of C3 annual cropland and C3 nitrogen-fixing cropland to C3 nitrogen-fixing cropland and C4 annual cropland have the largest effect, with RC of 53% and 53.9%, respectively. Based on the weighed mean, the replacement of secondary forested land by cropland contributed the most to the climate effect. The application of nitrogen fertilizer for C3 plant has greater contribution than C4 plants, while similar irrigation effects are found for different types of croplands. In addition to deforestation, we should pay attention to the temperature effect of urban land expansion and the transition of different types of croplands.

The results can enhance our understanding of LULCC's role in global climate system by revealing the dominant types of LULCC in modulating historical regional and global temperature, and also have great implications for guiding future model development efforts by identifying which types of LULCC are most uncertain in climate models.

## Declaration of Competing Interest

The authors declare that they have no known competing financial interests or personal relationships that could have appeared to influence the work reported in this paper

## Data Availability

Data will be made available on request.

## Acknowledgements

This research is supported by the National Key Research and Development Program of China (No. 2020YFA0608502) and the National Natural Science Foundation of China (No. 42077420).

## Supplementary materials

Supplementary material associated with this article can be found, in the online version, at doi:[10.1016/j.agrformet.2022.109232](https://doi.org/10.1016/j.agrformet.2022.109232).

## References

- Alkama, R., Cescatti, A., 2016. Biophysical climate impacts of recent changes in global forest cover. *Science* 351, 600–604. <https://doi.org/10.1126/science.aac8083>.
- Asselen, S., Verbburg, P.H., 2013. Land cover change or land-use intensification: simulating land system change with a global-scale land change model. *Glob. Chang. Biol.* 19, 3648–3667. <https://doi.org/10.1111/gcb.12331>.
- Betts, R.A., 2000. Offset of the potential carbon sink from boreal forestation by decreases in surface albedo. *Nature* 408, 187–190. <https://doi.org/10.1038/35041545>.
- Boone, A.A., Xue, Y., Sales, F.D., Comer, R.E., Hagos, S., Mahanama, S., Schio, K., Song, G., Wang, G., Li, S., Mechoso, C.R., 2016. The regional impact of Land-Use Land-cover Change (LULCC) over West Africa from an ensemble of global climate models under the auspices of the WAMME2 project. *Clim. Dyn.* 47, 3547–3573. <https://doi.org/10.1007/s00382-016-3252-y>.
- Burakowski, E., Tawfik, A., Ouimette, A., Lepine, L., Novick, K., Ollinger, S., Zarzycki, C., Bonan, G., 2018. The role of surface roughness, albedo, and Bowen ratio on ecosystem energy balance in the Eastern United States. *Agric. For. Meteorol.* 249, 367–376. <https://doi.org/10.1016/j.agrformet.2017.11.030>.
- Chen, L., Dirmeyer, P.A., 2016. Adapting observationally based metrics of biogeophysical feedbacks from land cover/land use change to climate modelling. *Environ. Res. Lett.* (11), 034002 <https://doi.org/10.1088/1748-9326/11/3/034002>.
- Doetterl, S., Stevens, A., Six, J., et al. Soil carbon storage controlled by interactions between geochemistry and climate. *Nat. Geosci.* 8, 780–783. <https://doi.org/10.1038/ngeo2516>.
- Dul, J., Ceyland, C., Jaspers, F., 2011. Knowledge workers' creativity and the role of the physical work environment. *Hum. Resour. Manage.* 50 (6), 715–734. <https://doi.org/10.1002/hrm.20454>.
- Forster, P., et al., 2007. Changes in atmospheric constituents and in radiative forcing. In: Solomon, S. et al. (Eds.), Climate change: the Physical Science basis. Contribution of Working Group to the Fourth Assessment Report of the Intergovernmental Panel On Climate Change. Cambridge University Press, Cambridge, pp. 130–234.
- Ghimire, R., Norton, U., Bista, P., Obour, A.K., Norton, J.B., 2017. Soil organic matter, greenhouse gases and net global warming potential of irrigated conventional, reduced-tillage and organic cropping systems. *Nutr. Cycling Agroecosyst.* 107, 49–62. <https://doi.org/10.1007/s10705-016-9811-0>.
- Good, A., 2018. Toward nitrogen-fixing plants. *Science* 359, 869–870. <https://doi.org/10.1126/science.aas8737>.
- Graesser, J., Aide, T.M., Grau, H.R., Ramankutty, N., 2015. Cropland/pastureland dynamics and the slowdown of deforestation in Latin America. *Environ. Res. Lett.* (10), 034017 <https://doi.org/10.1088/1748-9326/10/3/034017>.
- Gray, J.M., Frolking, S., Kort, E.A., Ray, D.K., Kucharik, C.J., Ramankutty, N., Friedl, M. A., 2014. Direct human influence on atmospheric CO<sub>2</sub> seasonality from increased cropland productivity. *Nature* 515, 398–401. <https://doi.org/10.1038/nature13957>.
- Guardia, G., Aguilera, E., Vallejo, A., Sanz-Cobena, A., Alonso-Ayuso, M., Quemada, M., 2019. Effective climate change mitigation through cover cropping and integrated fertilization: a global warming potential assessment from a 10-year field experiment. *J. Clean. Prod.* 241, 118307 <https://doi.org/10.1016/j.clepro.2019.118307>.
- Horton, D.E., Johnson, N.C., Singh, D., Swain, D.L., Rajaratnam, B., Daffenbaugh, N.S., 2015. Contribution of changes in atmospheric circulation patterns to extreme temperature trends. *Nature* 522, 465–469. <https://doi.org/10.1038/nature14550>.
- Houghton, R.A., Nassikas, A.A., 2017. Global and regional fluxes of carbon from land use and land cover change 1850–2015. *Global Biogeochem. Cycles* 31, 456–472. <https://doi.org/10.1002/2016GB005546>.
- Huang, B., Hu, X.P., Fuglstad, G., Zhou, X., Zhao, W., Cherubini, F., 2020. Predominant regional biophysical from recent land cover changes in Europe. *Nat. Commun.* 11, 1066. <https://doi.org/10.1038/s41467-020-14890-0>.
- Huang, K., Li, X., Liu, X., Seto, K.C., 2019. Projecting global urban land expansion and heat island intensification through 2050. *Environ. Res. Lett.* 14, 114037 <https://doi.org/10.1088/1748-9326/ab4b71>.
- Hurtt, G., Chini, L.P., Frolking, S., Betts, R., Feddema, J., Fischer, G., Fisk, J., Hibbard, K., Houghton, R., Janetos, A., 2011. Harmonization of land-use scenarios for the period 1500–2100: 600 years of global gridded annual land-use transitions, wood harvest, and resulting secondary lands. *Clim. Change* 109, 117–161. <https://doi.org/10.1007/s10584-011-0153-2>.
- Iturbide, M., Cutiéreze, J.M., Alves, L.M., et al., 2020. An update of IPCC climate reference regions for subcontinental analysis of climate model data: definition and aggregated dataset. *Earth Syst. Sci. Data* 12, 2959–2970. <https://doi.org/10.5194/ess-12-2959-2020>.
- Jiang, F., Xie, X., Liang, S., Wang, Y., Zhu, B., Zhang, X., Cheng, Y., 2021. Loess Plateau evapotranspiration intensified by land surface radiative forcing associated with ecological restoration. *Agric. For. Meteorol.* 311, 108669 <https://doi.org/10.1016/j.agrformet.2021.108669>.
- Jose, V.S., Sejian, V., Bagath, M., Ratnakaran, A.P., Lees, A.M., Al-Hosni, Y.A.S., Sullivan, M., Bhatta, R., Gaughan, J.B., 2016. Modelling of greenhouse gas emission from livestock. *Front. Environ. Sci.* 4, 1–10. <https://doi.org/10.3389/fenvs.2016.00027>.
- Kala, J., Hirsch, A.L., 2020. Could crop albedo modification reduce regional warming over Australis? *Weather Clim. Extrem.* 30, 100282 <https://doi.org/10.1016/j.wace.2020.100282>.
- Lawrence, D.M., Hurtt, G.C., Arneth, A., Brovkin, V., Calvin, K.V., Jones, A.D., Jones, C. D., Lawrence, P.J., de Noblet-Ducoudré, N., Pontratz, J., Seneviratne, S.I., Shevliakova, E., 2016. The Land Use Model Intercomparison Project (LUMIP) contribution to CMIP6: rational and experimental design. *Geosci. Model. Dev.* 9, 2973–2998. <https://doi.org/10.5194/gmd-9-2973-2016>.
- Lee, et al., 2011. Observed increase in local cooling effect of deforestation at higher latitudes. *Nature* 479, 384–387. <https://doi.org/10.1038/nature10588>.
- Leip, A., Billen, G., Garnier, J., Grizzetti, B., Lassaletta, L., Reis, S., Simpson, D., Sutton, M.A., de Vries, W., Weiss, F., Westhonenk, H., 2015. Impacts of European livestock production: nitrogen, sulphur, phosphorus and greenhouse gas emissions, land-use, water eutrophication and biodiversity. *Environ. Res. Lett.* 10, 115004 <https://doi.org/10.1088/1748-9326/10/11/115004>.
- Li, Y., Guan, K., Peng, B., Franz, T.E., Wardlow, B., Pan, M., 2020b. Quantifying irrigation cooling benefits to maize yield in the US Midwest. *Glob. Chang. Biol.* 16, 3065–3078. <https://doi.org/10.1111/gcb.15002>.
- Li, Y., Piao, S., Chen, A., Caias, P., Li, L.Z.X., 2020a. Local and teleconnected temperature effects of afforestation and vegetation greening in China. *Natl. Sci. Rev.* 7, 897–912. <https://doi.org/10.1093/nsr/nwz123>.
- Liao, W., Liu, X., Burakowski, E., Wang, D., Wang, L., Li, D., 2020. Sensitivities and response of land surface temperature to deforestation-induced biophysical changes in two global earth system models. *J. Clim.* 33, 8381–8399. <https://doi.org/10.1175/JCLI-D-19-0725.sl>.
- Liao, W., Rigden, A.J., Li, D., 2018. Attribution of local temperature response to deforestation. *J. Geophys. Res.* 123, 1572–1587. <https://doi.org/10.1029/2018JG004401>.
- Luyssaert, S., Caias, P., Piao, S.L., et al., 2010. The European carbon balance. Part 3: forests. *Glob. Chang. Biol.* 16, 1429–1450. <https://doi.org/10.1111/j.1365-2486.2009.02056.x>.
- Luyssaert, S., Jammet, M., Stoy, P.C., Estel, S., Pontratz, J., Ceschia, E., Churkina, G., Don, A., Erb, K., Ferlicoq, M., 2014. Land management and land-cover change have impacts of similar magnitude on surface temperature. *Nat. Clim. Chang.* 4, 389–393. <https://doi.org/10.1038/nclimate2196>.
- Mahmood, R., et al., 2013. Land cover changes and their biogeophysical effects on climate. *Int. J. Climatol.* 34, 929–953. <https://doi.org/10.1002/joc.3736>.
- Mueller, N.D., Butler, E.E., McKinnon, K.A., Rhines, A., Tingley, M., Holbrook, N.M., Huybers, P., 2016. Cooling of US Mid-west summer temperature extremes from cropland intensification. *Nature Climate Change.* 6, 317–322. <https://doi.org/10.1038/nclimate2825>.
- Myers-Smith, I.H., 2020. Complexity revealed in the greening of the Arctic. *Nat. Clim. Chang* 10, 106–117. <https://doi.org/10.1038/s41558-019-0688-1>.
- Noblet-Ducoudré, N., et al., 2012. Determining robust impacts of land-use-induced land cover changes on surface climate over North America and Eurasia: results from the first set of LUCID experiments. *J. Clim.* 25, 3261–3281. <https://doi.org/10.1175/JCLI-D-11-00338.1>.
- Oster, E., 2019. Unobservable selection and coefficient stability: theory and evidence. *J. Bus. Econom. Statist.* 37, 187–204. <https://doi.org/10.1080/07350015.2016.1227711>.
- Perugini, L., Caporaso, L., Marconi, S., Cescatti, A., Quesada, B., Noblet-Ducoudré, N., House, J.I., Arneth, A., 2017. Biophysical effects on temperature and precipitation due to land cover change. *Environ. Res. Lett.* 12, 053002 <https://doi.org/10.1088/1748-9326/aa6b3f>.
- Pugh, T., Arneth, A., Olin, S., Ahlström, A., Bayer, A., Goldewijk, K.K., Lindeskog, M., Schurgers, G., 2015. Simulated carbon emissions from land-use change are substantially enhanced by accounting for agricultural management. *Environ. Res. Lett.* (10), 124008 <https://doi.org/10.1088/1748-9326/10/12/124008>.
- Puma, M.J., Cook, B.I., 2010. Effects of irrigation on global climate during the 20th century. *J. Geophys. Res.* 115, D16120. <https://doi.org/10.1029/2010JD014122>.
- Rasmussen, C., Heckman, K., Wieder, W.R., et al. Beyond clay: towards an improved set of variables for predicting soil organic matter content. *Biogeochem. Lett.* 137, 297–306. <https://doi.org/10.1007/s10533-018-0424-3>.
- Schuur, E.A.G., et al., 2015. Climate change and the permafrost carbon feedback. *Nature* 520, 171–179. <https://doi.org/10.1038/nature14338>.
- Scott, C.E., et al., 2018. Impact on short-lived climate forcers increases projected warming due to deforestation. *Nat. Commun.* 9, 157. <https://doi.org/10.1038/s41746-017-02412-4>.
- Song, X.P., Hansen, M.C., Stehman, S.V., Potapov, P.V., Tyukavina, A., Vermote, E.F., Townshend, J.R., 2018. Global land change from 1982 to 2016. *Nature* 560, 639–643. <https://doi.org/10.1038/s41586-018-0411-9>.
- Stoy, P.C., 2018. Deforestation intensifies hot days. *Nat. Clim. Chang.* 8, 366–368. <https://doi.org/10.1038/s41558-018-0153-6>.
- Thiery, W., Davin, E.L., Lawrence, D.M., Hirsch, A.L., Hauser, M., Seneviratne, S.I., 2017. Present-day irrigation mitigates heat extremes. *J. Geophys. Res.* 122, 1403–1422. <https://doi.org/10.1002/2016JD025740>.
- Tran, D.X., Pla, F., Latorre-Carmona, P., Myint, S.W., Caetano, M., Kieu, H.V., 2017. Characterizing the relationship between land use/land cover change and land surface temperature. *ISPRS J. Photogramm. Remote Sens.* 124, 119–132. <https://doi.org/10.1016/j.isprsjpre.2017.01.001>.

- Trlica, A., Hutyra, L.R., Schaaf, C.L., Erb, A., Wang, J.A., 2017. Albedo, Land cover, and daytime surface temperature variation across an urbanized landscape. *Earth's Future* 11, 1084–1101. <https://doi.org/10.1002/2017EF000568>.
- Wang, J., Li, W., Ciais, P., Li, L.Z.X., Chang, J., Goll, D., Gasser, T., Huang, X., Devaraju, N., Boucher, O., 2021. Global cooling induced by biophysical effects of bioenergy crop cultivation. *Nat. Commun.* 12, 7255. <https://doi.org/10.1038/s41467-021-27520-0>.
- Wang, J., Vanga, S.K., Saxena, R., Orsat, V., Raghavan, V., 2018. Effect of climate change on the yield of cereal crops: a review. *Climate* 6, 41. <https://doi.org/10.3390/cli6020041>.
- Winckler, J., Lejeune, Q., Reick, C.H., Pongratz, J., 2019. Nonlocal effects dominate the global mean surface temperature response to the biogeophysical effects of deforestation. *Geophys. Res. Lett.* 46, 745–755. <https://doi.org/10.1029/2018GL080211>.
- Xia, W., Bowattc, S., Jia, Z., Newton, P., 2022. Offsetting  $\text{N}_2\text{O}$  emissions through nitrifying  $\text{CO}_2$  fixation in grassland soil. *Soil Biol. Biochem.* 165, 108528 <https://doi.org/10.1016/j.soilbio.2021.108528>.
- Yang, M., Nelson, F.E., Shikolmanov, N.I., Guo, D., Wan, G., 2010. Permafrost degradation and its environmental effects on the Tibetan Plateau: a review of recent research. *Earth Sci. Rev.* 103, 31–44. <https://doi.org/10.1016/j.earscirev.2010.07.002>.
- Yang, Q., Huang, X., Tang, Q., 2020. Irrigation cooling effect on land surface across China based on satellite observations. *Sci. Total Environ.* 705, 135984 <https://doi.org/10.1016/j.scitotenv.2019.135984>.
- Yu, L., Leng, G., 2022. Identifying the paths and contribution of climate impacts on the variation in land surface albedo over the Arctic. *Agric. For. Meteorol.* 313, 108772 <https://doi.org/10.1016/j.agrformet.2021.108772>.
- Yu, L., Leng, G., Python, A., 2022. Attribution of the spatial heterogeneity of Arctic surface feedback to the dynamics of vegetation, snow and soil properties and their interactions. *Environ. Res. Lett.* 17, 014036 <https://doi.org/10.1088/1748-9326/ac4631>.
- Zemp, D.C., Schleussner, C.-F., Barbosa, H.M.J., Rammig, A., 2017. Deforestation effects on Amazon forest resilience. *Geophys. Res. Lett.* (44), 6182–6190. <https://doi.org/10.1002/2017GL072955>.
- Zeng, Z., et al., 2017. Climate mitigation from vegetation biophysical feedbacks during the past three decades. *Nat. Clim. Chang.* 7, 432–436. <https://doi.org/10.1038/nclimate3299>.
- Zeng, Z., Wang, D., Yang, L., et al., 2021. Deforestation-induced warming over tropical mountain regions regulated by elevation. *Nat. Geosci.* 14, 23–29. <https://doi.org/10.1038/s41561-020-00666-0>.
- Zeng, Z., Zhao, F., Collatz, G.J., Kalnay, E., Salawitch, R.J., West, T.O., Guanter, L., 2014. Agricultural green revolution as a driver of increasing atmospheric  $\text{CO}_2$  seasonal amplitude. *Nature* 515, 394–397. <https://doi.org/10.1038/nature13893>.
- Zhai, J., Liu, R., Liu, J., Zhao, G., Huang, L., 2014. Radiative forcing over China due to albedo change caused by land cover change during 1990–2010. *J. Geog. Sci.* 24, 789–801. <https://doi.org/10.1007/s11442-014-1120-4>.
- Zhang, X., Tang, Q., Zheng, J., Ge, Q., 2013. Warming/cooling effects of cropland greenness changes during 1982–2006 in the North China Plain. *Environ. Res. Lett.* (8), 024038 <https://doi.org/10.1088/1748-9326/8/2/024038>.
- Zhou, D., Xiao, J., Froliking, S., Liu, S., Zhang, L., Cui, Y., Zhou, G., 2021. Croplands intensify regional and global warming according to satellite observations. *Remote Sens. Environ.* 264, 112585 <https://doi.org/10.1016/j.rse.2021.112585>.
- Zona, D., 2016. Long-term effects of permafrost thaw. *Nature* 537, 625–626. <https://doi.org/10.1038/537625a>.
- Zubizarreta-Gerendiain, A., Pukkala, T., Peltola, H., 2016. Effects of wood harvesting and utilization policies on the carbon balance of forestry under changing climate: a Finnish case study. *For. Policy Econ.* 62, 168–176. <https://doi.org/10.1016/j.forpol.2015.08.007>.